Two-dimensional thermal convection flow with variable viscosity and embedded boundaries

M. Uhlmann, A. Pinelli

Dept. Combustibles Fósiles, CIEMAT
Avda. Complutense 22, 28040 Madrid (Spain)
markus.uhlmann@ciemat.es

February 2003

Abstract

A two-dimensional model capable of simulating thermal convection flow in complex geometries has been implemented in a finite-difference setting and using a fictitious domain method of type "direct explicit forcing". The Boussinesq approximation is supposed to hold; the coupling between velocity and temperature fields is explicit; spatially varying viscosity is accounted for. The computation of a model for the thermally-induced flow in a three-chamber fuel tank reveals that the present method does not allow for sufficiently large time steps when the viscosity varies strongly.

Key Words: Thermal convection, variable viscosity, fictitious domain, direct forcing, finite-differences.

1 Physical model

We consider the Navier-Stokes equations and the temperature equation in the framework of the Boussinesq approximation and variable viscosity, viz.

$$\partial_t u_i + p_{,i} + u_{,j} u_{i,j} = \left(\nu \left(u_{i,j} + u_{j,i}\right)\right)_{,j} - g_i \alpha_T \Delta T \tag{1a}$$

$$u_{i,i} = 0 \tag{1b}$$

$$\partial_t T + u_{,j} T_{,j} = \kappa T_{,jj} \tag{1c}$$

subject to appropriate boundary conditions. Here u_i is a component of the fluid velocity, p the pressure divided by the reference fluid density and $\nu(T)$ the kinematic viscosity which is in turn a function of the fluid temperature T; g_i is a spatial component of the gravitational acceleration vector, α_T the (constant) coefficient of thermal expansion of the fluid, $\Delta T \equiv T - T_{ref}$ the temperature difference w.r.t. a reference temperature T_{ref} and κ the (constant) thermal diffusivity.

2 Numerical method

The present numerical method is based upon the one described in [1], developed for particulate flows. The main modifications undertaken for our present purposes concern the introduction of a non-uniform grid and the variable viscosity.

We employ an *incremental-pressure projection method* (cf. [2]) for splitting the system (1a-1b) into two fractional steps. Using an implicit scheme for the viscous terms and a three-step

low-storage Runge-Kutta method with explicit non-linear terms, the semi-discrete system can be written as follows:

$$\begin{aligned}
\frac{u_i^* - u_i^{k-1}}{\Delta t} &= 2\alpha_k \left(\nu(T^{k-1}) \left(u_{i,j}^*\right)\right)_{,j} - 2\alpha_k p_{,i}^{k-1} \\
&\quad +\gamma_k \left\{ -\left(u_j u_{i,j}\right)^{k-1} + \left(\nu(T^{k-1})\right)_{,j} u_{j,i}^{k-1} - g_i \alpha_T \Delta T^{k-1} \right\} \\
&\quad +\zeta_k \left\{ -\left(u_j u_{i,j}\right)^{k-2} + \left(\nu(T^{k-2})\right)_{,j} u_{j,i}^{k-2} - g_i \alpha_T \Delta T^{k-2} \right\} \\
&\quad +f_i^k \qquad (2a) \\
\phi_{,jj}^k &= \frac{u_{i,i}^*}{2\alpha_k \Delta t} \qquad (2b) \\
u_i^k &= u_i^* - 2\alpha_k \Delta t \phi_{,i}^k \qquad (2c) \\
p^k &= p^{k-1} + \phi^k \qquad (2d) \\
\frac{T^k - T^{k-1}}{\Delta t} &= 2\alpha_k \kappa T_{,jj}^k - \gamma_k u_j^k T_{,j}^{k-1} - \zeta_k u_j^{k-1} T_{,j}^{k-2} \qquad (2e)
\end{aligned}$$

where $k = 1, 2, 3$ is the Runge-Kutta step count (with the level $k = 3$ being equivalent to $n + 1$), u^* the predicted, intermediate velocity and the intermediate variable ϕ is sometimes called "pseudo-pressure". The following set of coefficients, first published in reference [3], was used since it leads to overall second-order temporal accuracy for both velocity and pressure in the case of constant viscosity [1]:

$$\alpha_k = \left\{ \frac{4}{15}, \frac{1}{15}, \frac{1}{6} \right\}, \quad \gamma_k = \left\{ \frac{8}{15}, \frac{5}{12}, \frac{3}{4} \right\}, \quad \zeta_k = \left\{ 0, -\frac{17}{60}, -\frac{5}{12} \right\}. \qquad (3)$$

Several details concerning this particular formulation of the system of equations (2) deserve further mention.

- The split of the viscous terms $(\nu(u_{i,j} + u_{j,i}))_{,j} = (\nu u_{i,j})_{,j} + \nu_{,j} u_{j,i}$ allows for an implicit treatment of the former part while the latter part—being constituted of cross-derivative terms—is treated by the same explicit method as the advection terms.

- The implicit projection step (2a) requires the solution of a two-dimensional system of type $(1 - \partial_x \nu \partial_x - \partial_y \nu \partial_y) u^* = r.h.s.$ for each velocity component which is performed by a first-order accurate ADI method as described in § A.

- The volume force term f_i^k in (2a) has been used to force Dirichlet boundary conditions upon the velocity field at selected internal points of the computational domain which coincide with solid boundaries. The corresponding method of direct forcing—previously used in [4–6]—has been described in detail for the present implementation in [1]. The technique for obtaining the value of the forcing term is explicit in nature and requires a relatively cheap "pre-prediction step", formally: $f_i^k = f_i^k(u^{k-1}, u^{k-2}, p^{k-1}, \nu(T^{k-1}))$.

- The Poisson problem for pseudo-pressure (2b) and the Helmholtz problem for temperature (2e) are presently solved by a direct method, using as a core solver the block-tridiagonal routine `BLKTRI` from FISHPACK.

- The update for the pressure variable (2d) does not include the usual second-order update term $(-\alpha_k \Delta t \, \nu \nabla^2 \phi^k)$ in the present case.

- The coupling between velocity/pressure and temperature is explicit in the way that the temperature is lagging by one Runge-Kutta sub-step, i.e. the solution for velocity is explicit in temperature and the temperature is computed using the most recent solution of velocity for its advection.

The discretization of the spatial operators is performed using fully central second-order finite-differences as described in [7].

The functional dependence of viscosity upon temperature has been implemented by means of cubic spline interpolation from tabulated data in the relevant range of $0 - 50°C$.

Boundary conditions for pseudo-pressure are needed for the solution of the Poisson equation (2b). We use homogeneous Neumann conditions.

3 Results

The mapping function used for accumulating grid-nodes near the boundaries is monotone increasing from 0 to 1 and reads:

$$g(\xi) = \frac{1 + \tanh(2\alpha(2\xi - 1)\pi)}{2\tanh(2\alpha\pi)} \quad 0 \leq \xi \leq 1 \quad . \tag{4}$$

Therefore, we simply generate a uniform grid ξ with unit length and apply $x = g(\xi)$, then rescale the domain such that it has the desired dimension.

3.1 Lid-driven cavity flow

The lid-driven cavity has been used extensively for validation of flow solvers in the literature. The flow develops inside a closed square cavity, $\Omega = [0, 1] \times [0, 1]$, with the top boundary moving at constant speed, cf. figure 1. The boundary conditions are therefore:

$$\mathbf{u}(0, y) = 0,\ \mathbf{u}(1, y) = 0,\ \mathbf{u}(x, 0) = 0,\ u(x, 1) = 1,\ v(x, 1) = 0, \tag{5}$$

while the adequate condition for pressure is homogeneous Neumann over the full boundary. For this case the viscosity is taken to be constant.

It should be noted that in the framework of a staggered grid arrangement, special care needs to be taken at the corner points $\mathbf{x} = (0, 1)$ and $\mathbf{x} = (1, 1)$ in order to satisfy both, the Dirichlet condition for velocities and the condition that $\partial u/\partial x = 0$ and $\partial v/\partial y = 0$ there; otherwise, a non-zero value for the pseudo-pressure is obtained which drives the pressure to non-physical values at these corner points.

Figure 2 shows velocity profiles of our computations pertaining to uniform and tanh-stretched grids with 100×100 nodes. The steady state was reached by convergence of the maximum norm of the residual below 10^{-7}. Both results are nearly identical and correspond reasonably with results from Ghia *et al.* [8] at the present Reynolds number of $Re = 400$.

3.2 Thermal convection in a square cavity

Here, the domain is again $\Omega = [0, 1] \times [0, 1]$. The walls are all no-slip. A temperature gradient between the left and right isothermal walls drives the motion. The top and bottom walls are adiabatic, i.e. no normal gradient of temperature, cf. figure 3.

The Prandtl and Rayleigh numbers are defined as follows:

$$Pr \equiv \frac{\nu}{\kappa}, \qquad Ra \equiv \frac{\alpha_t \, |\mathbf{g}| \, \Delta T \, L^3}{\nu \, \kappa} \quad , \tag{6}$$

with ΔT being the temperature gradient across the domain and L the characteristic length, i.e. the domain size here. The viscosity is again constant $\nu = 1$ and for the current test we used $Pr = 0.71$, $Ra = 1000$ and a grid of 100×100 nodes with a stretching of $\alpha = 0.4$.

The results for the steady solution are shown in figures 4-6 and correspond qulitatively with those of reference [9].

α_t	=	7.4×10^{-4}
g_1	=	0
g_2	=	9.81
κ	=	7.56×10^{-8}
T_w	=	2.6
T_{ref}	=	T_w
$T(t=0)$	=	50
$\nu(T=2.6)$	=	6.42×10^{-1}
$\nu(T=3.125)$	=	4.94×10^{-1}
$\nu(T=5.25)$	=	2.96×10^{-1}
$\nu(T=10.25)$	=	1.58×10^{-1}
$\nu(T=15.25)$	=	4.44×10^{-2}
$\nu(T=20.125)$	=	1.93×10^{-2}
$\nu(T=50)$	=	8.40×10^{-4}

Table 1: Physical parameters of the problem of thermally-induced convection in a fuel tank.

3.3 A model for a cross-section through a fuel tank

Physical parameters of the problem are given in table 1, the geometry is shown in figure 7. It should be noted that the geometry is symmetric w.r.t. the vertical centerline. However, the present computations were carried out with the computational domain covering the full cross-section of the tank such as to allow for possible non-symmetric or non-mirror-symmetric motions to develop.

The grid was generated with hyperbolic-tangent stretching (4) in each of the three tanks and in both coordinate directions.

Unfortunately, it turned out that the maximum time-step for a stable integration of the equations was prohibitively small compared to the long integration times we are aiming at. As an example, using a 400×200 grid and a stretching factor of $\alpha = 0.4$, the time step needed to be restricted to $\Delta t = 0.0003$, which is several magnitudes below the time step limit imposed by the traditional CFL condition. The reason for this phenomenon is not quite clear at the moment. When the viscosity was set equal to the viscosity of the fuel at $T = 50$, then the time step with $CFL = 0.5$ is stable.

Nevertheless, we performed some short-time computations of the full problem, i.e. including variable viscosity, whose results are shown in figure 8. It should be noted that the above mentioned grid has the first point at a wall-distance of 0.003 and the eighth point at 0.05 in both, the horizontal and the vertical direction. After the short integration time of 160 (i.e. less than three minutes of physical time) the temperature has virtually not changed over the domain. The velocity field (figure omitted) shows nothing but the buoyant movement due to a thin thermal boundary layer at the two exterior vertical walls which is growing in time while in the central compartment the fluid is nearly at rest.

4 Conclusion

A two-dimensional model capable of simulating thermal convection flow in complex geometries has been implemented in a finite-difference setting and using a fictitious domain method of type "direct explicit forcing". The Boussinesq approximation is supposed to hold. The coupling between velocity and temperature fields is explicit; the fact that viscosity varies spatially as a function of temperature is accounted for by adapting the semi-implicit projection method accordingly.

The method was validated for two classic cases: lid-driven cavity flow and thermal convection in a square cavity.

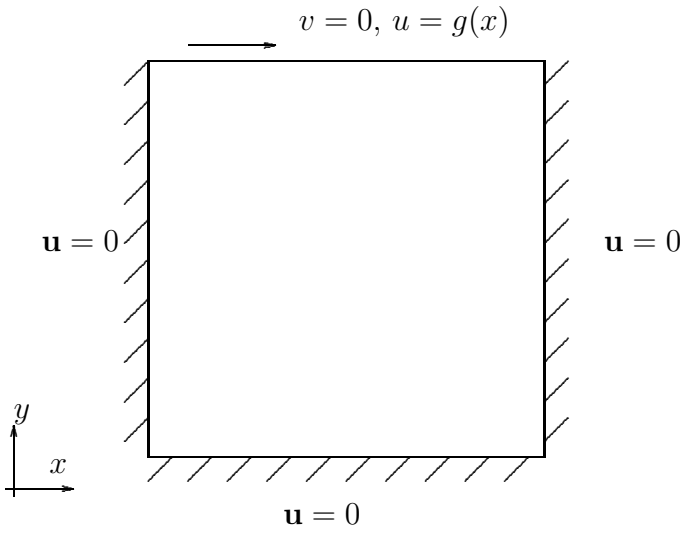

Figure 1: Schematic of the lid-driven cavity configuration.

The computation of a model for the thermally-induced flow in a three-chamber fuel tank has revealed that the present method does not allow for sufficiently large time steps (as compared to long integration times) when the viscosity varies strongly in space.

References

[1] M. Uhlmann. First experiments with the simulation of particulate flows. unpublished report available under the URL: `www.ciemat.es/sweb/comfos/personal/uhlmann`, 2003.

[2] D.L. Brown, R. Cortez, and M.L. Minion. Accurate projection methods for the incompressible Navier-Stokes equations. *J. Comput. Phys.*, 168:464–499, 2001.

[3] M.M. Rai and P. Moin. Direct simulation of turbulent flow using finite-difference schemes. *J. Comput. Phys.*, 96:15–53, 1991.

[4] R. Verzicco, J. Mohd-Yusof, P. Orlandi, and D. Haworth. Les in complex geometries using boundary body forces. *CTR Proc. Summer Prog.*, pages 171–186, 1998.

[5] E.A. Fadlun, R. Verzicco, P. Orlandi, and J. Mohd-Yusof. Combined immersed-boundary finite-difference methods for three-dimensional complex flow simulations. *J. Comput. Phys.*, 161:35–60, 2000.

[6] J. Kim, D. Kim, and H. Choi. An immersed-boundary finite-volume method for simulations of flow in complex geometries. *J. Comput. Phys.*, 171:132–150, 2001.

[7] O.V. Vasilyev. High order finite difference schemes on non-uniform meshes with good conservation properties. *J. Comput. Phys.*, 157:746–761, 2000.

[8] V. Ghia, K.N. Ghia, and C.T. Shin. High-Re solutions for incompressible flow using the Navier-Stokes equations and a multi-grid method. *J. Comput. Phys.*, 48:387–411, 1982.

[9] G. de Vahl Davis and I.P. Jones. Natural convection in a square cavity: A comparison exercise'. *Int. J. Num. Meth.*, 3:227–248, 1983.

[10] C.G. Hirsch. *Numerical computation of internal and external flows.* J. Wiley, 1990.

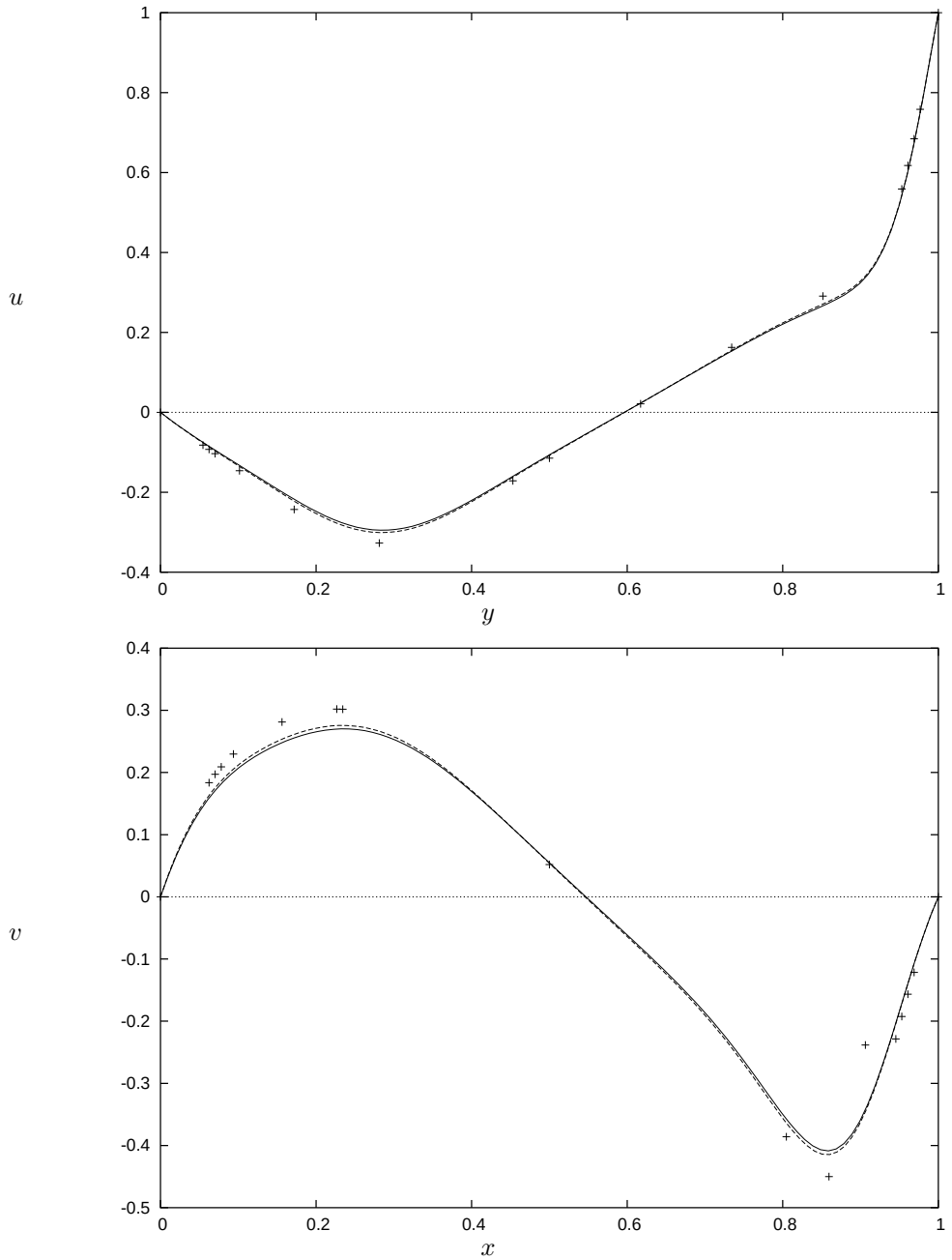

Figure 2: Numerical results for the lid-driven cavity case at $Re = 400$: (a) y-profile of the x-velocity at $x = 0.5$; (b) x-profile of the y-velocity at $y = 0.5$. The symbols correspond to the reference solution of Ghia *et al.* [8], the lines are the present results with a 100×100 grid and: ——— , uniform distribution; - - - - , tanh-stretching with stretching factor of $\alpha = 0.1$.

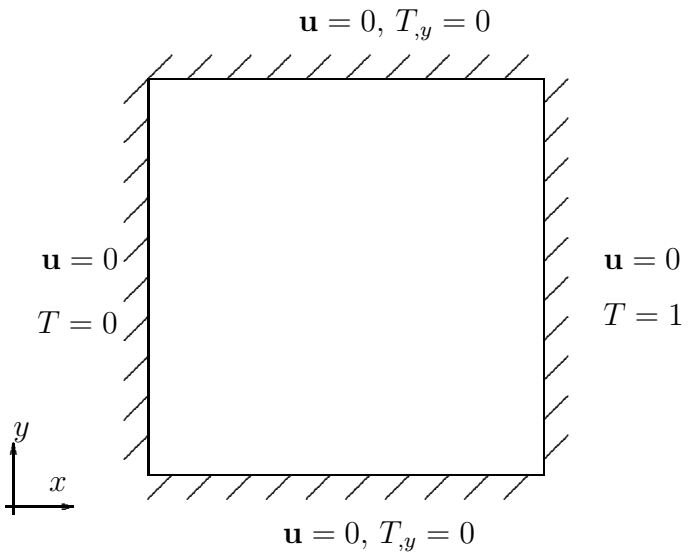

Figure 3: Schematic of the thermal cavity configuration.

A Approximate factorization method

The predictor step for velocity (2a) can be rewritten as

$$u_i^* - u_i^{k-1} = C(S_x + S_y)u_i^* + F_i \tag{7}$$

for convenience, defining:

$$\begin{aligned}
C &= 2\alpha_k \Delta t && \text{(8a)}\\
S_x &= \partial_x \nu(T^{k-1})\partial_x && \text{(8b)}\\
S_y &= \partial_y \nu(T^{k-1})\partial_y && \text{(8c)}\\
F_i &= \Delta t \left\{ -\gamma_k \left(u_j u_{i,j}\right)^{k-1} - \zeta_k \left(u_j u_{i,j}\right)^{k-2} \right. && \text{(8d)}\\
&\quad +\gamma_k \left(\nu(T^{k-1})\right)_{,j} u_{j,i}^{k-1} + \zeta_k \left(\nu(T^{k-2})\right)_{,j} u_{j,i}^{k-2} && \text{(8e)}\\
&\quad \left. -2\alpha_k p_{,i}^{k-1} - \gamma_k g_i \alpha_T \Delta T^{k-1} - \zeta_k g_i \alpha_T \Delta T^{k-2} + f_i^k \right\}. && \text{(8f)}
\end{aligned}$$

The Douglas-Rachford scheme (cf. [10, p.440]) consists in the following factorization of equation (7)

$$(1 - CS_x)\,(1 - CS_y)u_i^* = u_i^{k-1} + F_i + \mathcal{O}(\Delta t^2) \quad , \tag{9}$$

leading to a first-order-time-accurate solution in two separate one-dimensional steps:

$$\begin{aligned}
(1 - CS_x)u_i' &= (1 + CS_y)u_i^{k-1} + F_i\,, && \text{(10a)}\\
(1 - CS_y)u_i^* &= u_i' - CS_y u_i^{k-1}\,. && \text{(10b)}
\end{aligned}$$

The intermediate solution u_i' does not have a physical meaning and is later discarded. However, one needs to apply consistent boundary conditions to the first sweep in order to obtain the expected solution after the second sweep. This can be seen simply by rewriting the second sweep at the boundary as follows:

$$(u_i')_{L,R} = (1 - CS_y)\,(u_i^*)_{L,R} + CS_y \left(u_i^{k-1}\right)_{L,R} \quad , \tag{11}$$

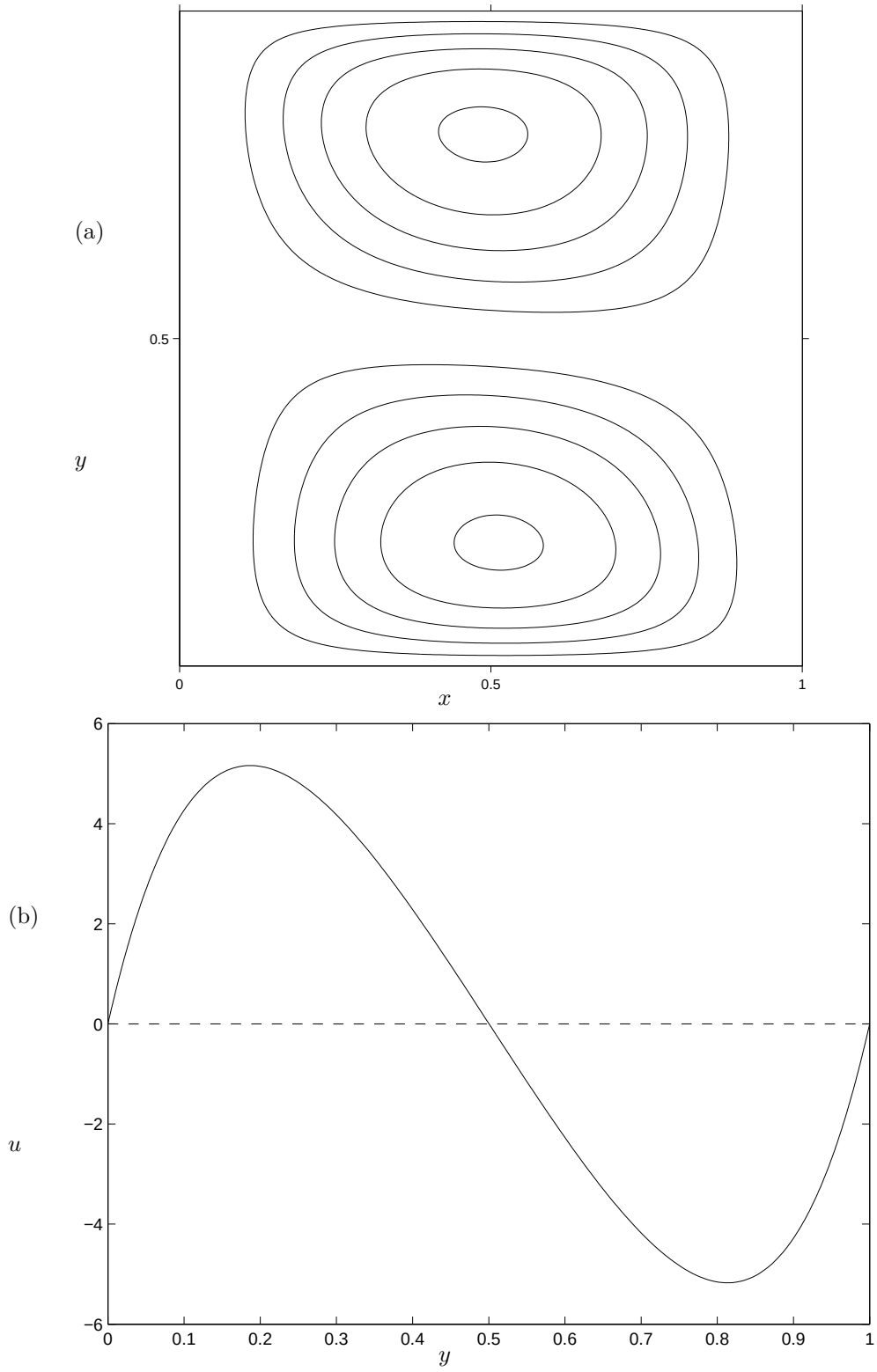

Figure 4: Numerical results for the thermally driven cavity case at $Ra = 1000$, obtained with a 400×400 grid and a stretching factor of $\alpha = 0.4$: x-velocity component. (a) iso-values at -5:1:5; (b) profile at $x = 0.5$.

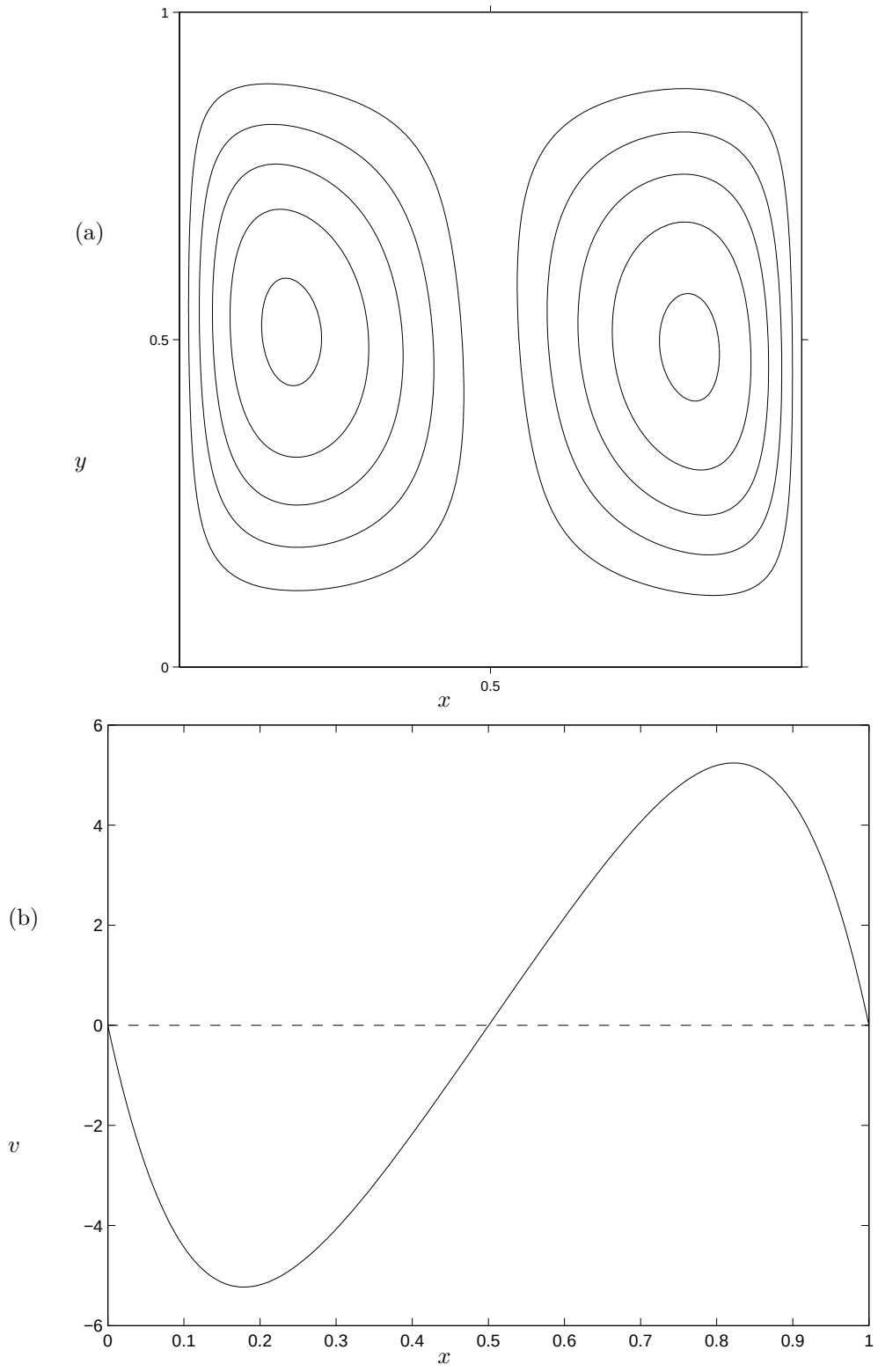

Figure 5: As figure 4, but showing the y-component of velocity: (a) iso-values at -5:1:5; (b) profile at $y = 0.5$.

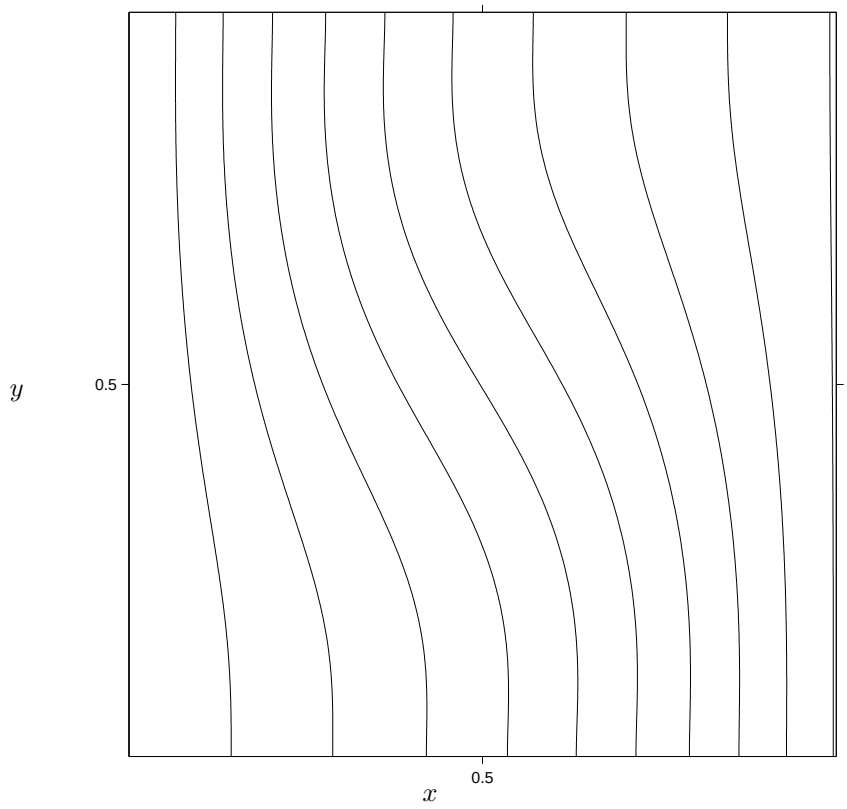

Figure 6: As figure 4 but showing iso-values of the temperature at 0:.1:1.

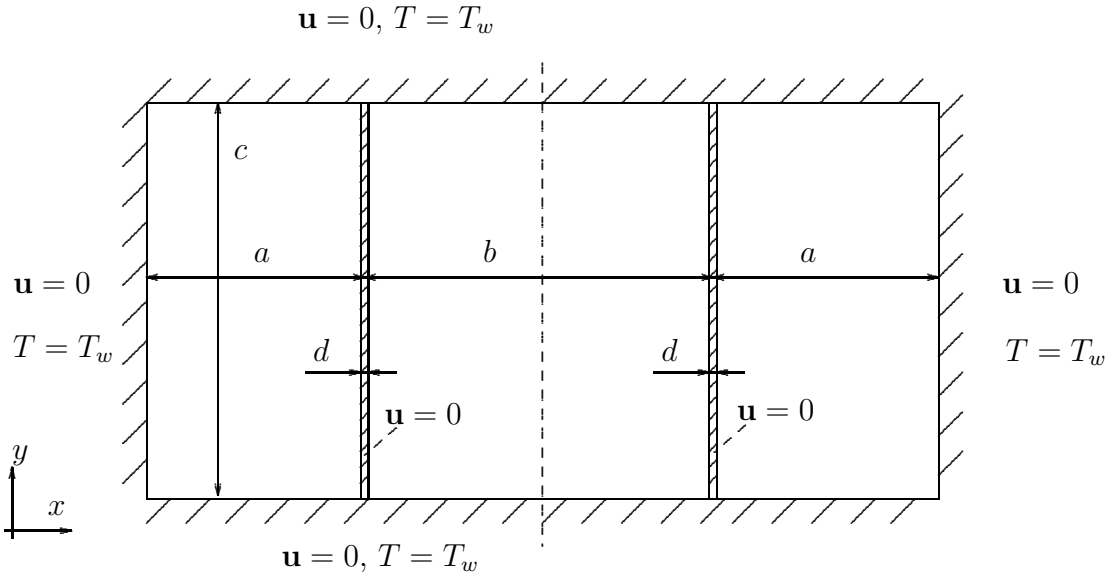

Figure 7: Schematic of the fuel tank configuration which is symmetric w.r.t. the vertical dashed line. The geometrical parameters are: $a = 9.6$, $b = 15.2$, $c = 18.7$; the wall thickness was set to $d = 0.2$ for the present computations.

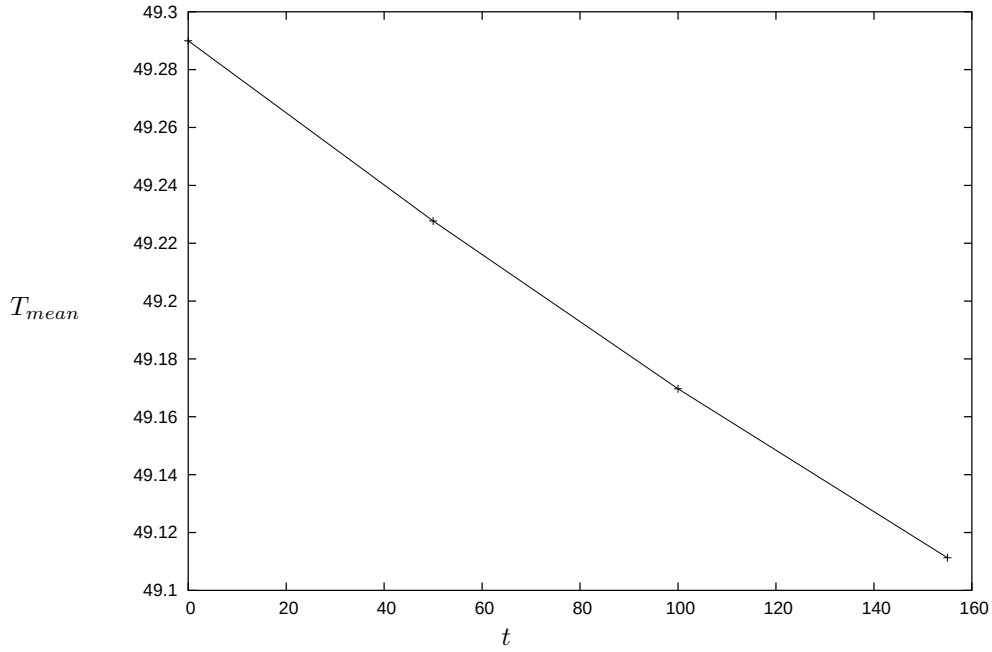

Figure 8: Numerical results for the fuel tank model with variable viscosity, a grid of 400×200 nodes with stretching factor $\alpha = 0.4$ and a time step of 0.0003. The plot shows the mean temperature as a function of time.

where $()_{L,R}$ refers to values at the left and right boundary of the computational domain. Therefore, the adequate boundary condition at the extrema of the first sweep is obtained by a combination of the operator along those boundaries applied to the previous solution u_i^{k-1} and the desired boundary conditions u_i^*. Both quantities are available in the case of Dirichlet boundary conditions and a grid which is centered w.r.t. the physical boundary. The conclusion for a staggered grid is that one needs to perform first a sweep in the non-staggered direction and subsequently in the staggered one, i.e. for the x-velocity sweep first in y then in x and vice versa for the y-velocity. In the case of a homogeneous Neumann condition, it should be chosen to lie along the staggered boundary (i.e. for the x-velocity: the lines $x = cst$). This means that we are presently neither capable to simulate two perpendicular Neumann conditions for a single velocity component nor Neumann conditions for both components at a single boundary. Fortunately, the present cases of interest do not fall into either class.